Energy Flows in the Forward Region at HERA

Mark Sutton[1]

Transfer Report - February 1996

Abstract

This report begins with a brief (and somewhat inadequate) review of the physics relevent to Neutral Current Deep Inelastic Scattering at HERA. Following this, generator level results for the Transverse Energy Flow for three new versions of the standard Monte Carlos used at the HERA experiments are presented. It is demonstrated that the new versions of the Monte Carlos - notably those based on traditional DGLAP dynamics - are now able to offer a reasonable description of the experimental data in the low x_{Bj} region.

[1]University College London

Contents

1 Deep Inelastic Scattering

During the 1960s, the accumulation of data on hadronic resonances seemed to suggest that the observed meson and baryon states were not in fact fundamental particles, but consisted instead of of some other, more elementary particles.

In 1964 Gell-Mann and Zweig postulated that these more fundamental particles consisted of a family of spin half particles which they called *quarks* each carrying fractional charge and transforming under an $SU(3)$ symmetry which they called "flavour" [1].

According to them each hadron was comprised of either three quarks (baryons) or a quark and an anti-quark (mesons). Thus the properties of the observed hadrons were explained by the flavours of their constituent quarks.

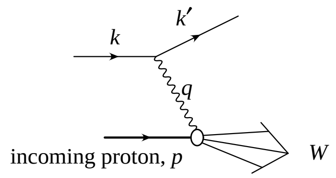

Figure 1: Deep inelastic lepton-proton scattering

The lack of any directly observable evidence of the quarks however, lead many to regard quarks as nothing but mathematical entities, rather than actual particles. However, strong evidence to support the quark model came in 1968 from Deep Inelastic Scattering (DIS) experiments at SLAC - where incident electrons were scattered with large momentum transfer off a fixed hydrogen target causing the protons to break up (fig. 1). This was the observation of Bjorken Scaling - the proton structure function becoming independent of the momentum transfer as it is increased - which showed that at large momentum transfer the lepton behaved as if it were scattering off essentially free point-like constituents within the proton. These constituents (named "partons" by Feynman) were soon identified with the quarks of Gell-Mann and Zweig.

Despite this apparent success of the so-called Quark-Parton Model (QPM) there were still important problems, notably the apparent violation of the Pauli exclusion principle required to construct the Δ^{++} resonance from three up quarks in the same spin state.

Consequently, the experimental observation of Bjorken scaling when taken with proof of the renormalizability of gauge theories (particularly the $U(1)$ gauge theory of Quantum Electrodynamics - QED) and the related realisation that the coupling of some non-abelian theories could be made to run, naturally lead to the idea that the strong interaction could also be explained by a gauge theory, but describing the dynamics of hadronic constituents rather than the hadrons themselves, with the interactions between the quarks being mediated by 8 massless gauge bosons which were called gluons.

These were required to satisfy the invariance of the lagrangian under local $SU(3)$ transformations - this extra degrre of freedom, known as "colour", being necessary in order to render the hadronic wavefunctions anti-symmetric as required.

The running coupling of the resulting theory of Quantum Chromodymamics (QCD) means that the strength of the interaction between the quarks increases at large distances (small momentum transfer) such that at very small distances (large momentum transfer) the quarks behave as if essentially free, non-interacting fermions. This then provides an explaination as to how the quarks are permanently confined within the hadrons, yet behave as if free particles when probed at high momentum in deep inelastic scattering experiments. This property, known as *asymptotic freedom* means that in the high energy limit, we are able to calculate quantities which do not depend on the long distance behaviour of the theory as a peturbative expansion in the coupling α_s.

Therefore we find that cross-sections can be *factorized* into a hard, peturbatively calculable component and a soft, non-peturbative component represented by the convolution

$$\sigma = \sum_i f_i^h * \sigma_i \tag{1}$$

where the sum is over all partons within the relevant hadron h. The quantities f_i^h are known as *parton distribution functions* and contain information on the soft part of the interaction, whereas the σ_i contain the dynamics of the hard scattering and are calculable in peturbative QCD.

The f_i^h can then be thought of as the probability of finding parton i in hadron h with the relevant fraction of the hadronic momentum. The cross sections σ_i are independent of the interacting hadron and the parton distributions are independent of the hard scattering and are therefore thought to be the same for all interactions involving a hadron of type h. This property is known as *hadron universality.*

These properties will be necessary later in our discussion of the calculation of observable quantities.

1.1 Kinematics

Before going on to describe the Quark Parton Model in more detail, it is first useful to examine the kinematics of DIS.

In a DIS event, the incoming high energy lepton scatters off the proton via the exchange of a virtual photon γ^*. In a neutral current (NC) event the exchanged boson can of course also be a Z^0 however in that case we must also consider both the contributions from the γ^* and Z^0 together with the interference term. Similarly in a charged current (CC) event the exchanged boson is a $W^\pm$ and the

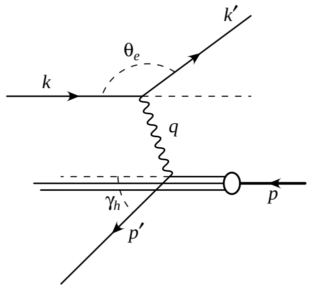

Figure 2: The kinematic variables of deep inelastic scattering

final state lepton a neutrino which can only be detected via missing energy and momenta. Consequently, for this simplified discussion we will only consider the vector component of the electroweak current - specifically that of the photon.

If the value of the momentum transfer between the lepton and proton is sufficiently high, the exchanged boson is able to resolve the pointlike constituents within the proton.

This is illustrated in figure 2 where k and k' are the incoming and scattered lepton 4-momenta respectively and p is the 4-momentum of the incoming proton.

The 4-momentum transfer q between lepton and the constituent quark is given by

$$q = k - k' \tag{2}$$

such that the exchanged boson is space-like ($q^2 < 0$) and as such it is convenient to introduce the positive quantity

$$Q^2 \equiv -q^2 \approx 2k.k' \tag{3}$$

(where we have neglected the mass of the scattering lepton).

At high momentum transfer to a good approximation we may also neglect the mass of the incident proton then the invariant mass of the final hadronic state W^2 is given by

$$W^2 = (p+q)^2 \approx 2p.q + q^2 \equiv 2p.q - Q^2. \tag{4}$$

It is also useful to define the dimensionless invariant quantities x and y given by

$$x \equiv \frac{Q^2}{2p.q} \tag{5}$$

$$y \equiv \frac{p.q}{p.k} \tag{6}$$

such that $0 \leq x, y \leq 1$ in terms of which we obtain

$$W^2 = Q^2 \left[\frac{1}{x} - 1\right]. \tag{7}$$

It is also informative to consider the total invariant mass of the colliding system s. This is given by

$$s = (p+k)^2 \approx 2p.k = \frac{Q^2}{xy} \tag{8}$$

and consequently at fixed s only two of the three invariants x, y or Q^2 are actually independent.

1.2 The Quark Parton Model

In the parton model we assume the interaction at the hadron vertex to be an elastic scatter from an effectively point-like constituent within the proton. As such the total cross section will be given in terms of the cross section for elastic scattering off a parton and the probability of finding such a parton within the proton as in equation (1).

We will find it necessary to work in the so-called "infinite momentum frame" where the proton momentum is large such that all the constituents move along the proton direction and all masses can be neglected. In this frame the proton will appear to the incident lepton Lorentz contracted to a thin disc, and furthermore the time dilation of the proton will mean that any parton-parton interactions within the proton occur on a large time scale compared to the parton-photon interaction of the hard scatter. This is the so-called "impulse approximation" and is very important in the parton model.

We now say a little more about scaling in DIS. The cross-section can be written as the product of a leptonic tensor $L^{\mu\nu}$ and a hadronic tensor $W^{\mu\nu}$,

$$\frac{\mathrm{d}^2\sigma}{\mathrm{d}\Omega \mathrm{d}E'} \sim L^{\mu\nu} W_{\mu\nu} \tag{9}$$

where Ω is the solid angle into which the lepton is scattered and we have averaged over initial and summed over final spins (and neglected flux factors and so on for clarity at this point). The leptonic vertex knows nothing about the hadronic interaction and as such is completely calculable from electroweak theory. Our ignorance about the process lies entirely within the hadronic vertex which has a non-peturbative component and is thus completely unknown. It is however possible to restrict the form of the hadronic tensor using symmetry and current conservation arguments (see for instance [2]). In this case we obtain the most general form for the vector coupling to the photon

$$W^{\mu\nu} = W_1 \left(-g^{\mu\nu} + \frac{q^\mu q^\nu}{q^2}\right) + \frac{1}{M^2} W_2 \left(p^\mu - \frac{(p.q)q^\mu}{q^2}\right)\left(p^\nu - \frac{(p.q)q^\nu}{q^2}\right) \tag{10}$$

where the $W_{1,2}$ are dimensionless functions of the lorentz scalars which can be constructed from the 4-momenta present at the hadronic vertex, for instance $W_{1,2}(\nu, Q^2)$ where

$$\nu \equiv \frac{p.q}{M} \tag{11}$$

which in the proton rest frame is given by

$$\nu = E_e - E_e' \tag{12}$$

and can thus be thought of as the energy given to the proton in its own rest frame. [2]

Using the form of the lepton tensor, it is then reasonably straightforward to show [2] that in the proton rest frame the cross section can be written as

$$\frac{\mathrm{d}^2\sigma}{\mathrm{d}\Omega \mathrm{d}E'} = \frac{\alpha^2}{4E_e \sin^4(\theta/2)} \left[2W_1(\nu, Q^2) \sin^2\left(\frac{\theta}{2}\right) + W_2(\nu, Q^2) \cos^2\left(\frac{\theta}{2}\right) \right]. \tag{13}$$

So far our discusion has been completely general, and not specific to the parton model, There is precious little physics in all of this - what we have done is merely to state the restrictions on any forms of the structure functions. In order to proceed further it is necessary to impose our assumptions about the nature of the virtual photon-proton interaction. If we consider the interaction to be that of

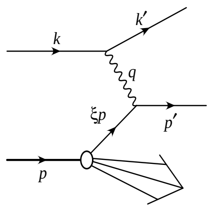

Figure 3: Parton level Deep Inelastic Scattering

an *elastic* scatter from a parton i within the proton (fig. 3), then in the impulse approximation we neglect the transverse momentum of the parton within the proton such that the parton carries a fraction ξ_i of the proton's longitudinal momentum such that $p_i = \xi_i p$, and further, that the parton is approximately on-shell both before and after the interaction. This then gives us

$$(\xi_i p + q)^2 \approx 2\xi_i p.q + q^2 \approx 0 \tag{14}$$

[2]As y is related to ν by $M\nu = (p.k)y$ then y can similarly be interpreted as the *fraction* of the incoming lepton energy in the proton's rest frame

which means that (in the impulse approximation)

$$\xi_i = \frac{Q^2}{2p.q} = x \tag{15}$$

and we see that in the parton model the Bjorken scaling variable x can be identified with the longitudinal momentum fraction carried by the struck parton.

In order to calculate the cross section it is then necessary to multiply the cross section for the elastic parton-photon scatter by the probability density $f_i(x)$ of finding a parton of type i with a momentum fraction between x and $x + \delta x$ summed over all partons within the proton. These probability density functions however, are not predicted by the parton model. They must obey certain sum rules to satisfy the number of, for example, valence quarks within the proton as predicted by the Gell-Mann and Zweig quark model.

Consequently, if we integrate over all possible parton momenta and sum over all partons we should obtain the following,

$$\sum_i \int_0^1 \mathrm{d}x \; (xp) f_i(x) \;=\; p, \tag{16}$$

$$\sum_i \int_0^1 \mathrm{d}x \; x f_i(x) \;=\; 1. \tag{17}$$

Once the parton distribution functions $f_i(x)$ have been identified, it is possible to compute the previously unknown structure functions $W_{1,2}(\nu, Q^2)$. These are then found to be

$$\nu W_2(\nu, Q^2) \to F_2(x) \;=\; \sum_i e_i^2 x f_i(x) \quad \text{and} \tag{18}$$

$$M W_1(\nu, Q^2) \to F_1(x) \;=\; \frac{1}{2x} F_2(x) \tag{19}$$

where the $F_{1,2}(x)$ depend *only on the scaling variable* x and not on the momentum transfer Q^2. Consequently the differential cross-section in terms of these structure functions also scales,

$$\frac{\mathrm{d}^2\sigma}{\mathrm{d}x\mathrm{d}y} = \frac{4\pi\alpha^2 s}{Q^4} \left[(1-y)F_2(x) + \frac{1}{2}y^2 \; 2xF_1(x) \right]. \tag{20}$$

This is what we previously referred to as Bjorken Scaling, and it was the observation of this behaviour at SLAC and the so-called Callan-Gross relation [3]

$$F_2(x) = 2xF_1(x) \tag{21}$$

which was one of the initial successes of the quark parton model.

At higher energies however, it is found that the cross-sections in fact deviate slightly from the predictions of scaling, and in order to understand how this occurs, we will find it necessary to modify the QPM to include the predictions of QCD.

1.3 QCD Corrections to the Parton Model

If we consider equation (16) then we see that the total momentum carried by the partons within the proton must sum to give the total proton momentum. Similarly we see that the structure function $F_2(x)$ sums the momentum fractions of all the *charged* partons. Consequently in the simple parton model where the proton is considered to consist simply of charged quarks then we would expect

$$\int_0^1 \mathrm{d}x \ F_2(x) = 1. \tag{22}$$

However, upon performing this integral experimentally, we find that the integral amounts to only a little over 0.5 of the proton's total momentum.

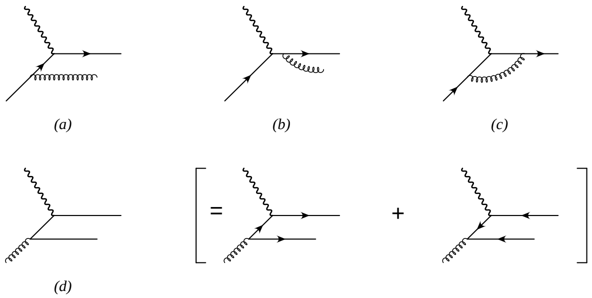

Figure 4: Some $\mathcal{O}(\alpha_s)$ Corrections to Deep Inelastic scattering: (a) and (b) QCD Compton Scattering, (c) vertex loop correction and (d) boson-gluon fusion. ($\mathcal{O}(\alpha_s)$ loop corrections to to fermion propagators are not shown.)

Consequently we see this as evidence of the existence of *uncharged* partons within the proton carrying $\sim 50\%$ of the proton momentum. These we identify

with the gluons - the 8 gauge bosons of QCD. The inclusion of gluons immediately leads to the possiblity that a quark can radiate gluons either before of after the hard interaction. Furthermore, a gluon could produce a $q\bar{q}$ pair, of which either could interact with the virtual photon.

So we would expect the inclusion of QCD interactions lead immediately to the prediction that scaling is violated. This was experimentally confirmed by the observation of a logarithmic dependence on Q^2 of $F_2(x, Q^2)$ [4] and was one of the first major successes of peturbative QCD. Some of the $\mathcal{O}(\alpha_s)$ QCD corrections to DIS are shown in figure 4.

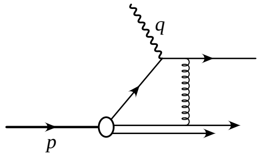

Figure 5: A Higher Twist Correction to DIS at $\mathcal{O}(\alpha_s)$

Again, if we use the impulse approximation then interactions between separate partons can be neglected, however there also exist so-called "higher twist" contributions of the form shown in figure 5 which can, in principle, destroy the factorization of the cross-section into hard (peturbative) and soft (non-peturbative) contributions. These however, it is believed, are suppressed by $\mathcal{O}(1/Q^2)$ [5] and can be neglected at high momentum transfers.

1.3.1 The Running Coupling

From Renormalization arguments we obtain the following expression for the running of the coupling constant α_s with some external energy μ^2

$$\frac{\mathrm{d}\alpha_s(\mu^2)}{\mathrm{d}\ln\mu^2} = \beta(\alpha_s^2). \tag{23}$$

To leading order, using the appropriate form for the Callan-Symanzik β function $\beta(\alpha_s^2) = -b_0\alpha_s^2(\mu^2)$ where $b_0 = (33 - 2N_f)/12\pi$ and N_f is the number of active flavours [6] we obtain the following

$$\alpha_s(\mu^2) = \frac{1}{b_0 \ln(\mu^2/\Lambda^2)} \tag{24}$$

where we have eliminated the dependence on the unphysical renormalization scale by the introduction of the dimensionful constant Λ.

From this we see that the coupling constant becomes asymmtotically large as $\mu \to \Lambda$ and consequently Λ can be considered as the scale at which QCD becomes "strong" and the peturbative method breaks down.

2 QCD Evolution Equations

2.1 The Leading Log (DGLAP) Approximation

In QCD each parton has to be considered as being surrounded by a cloud of virtual particles, which are constantly being created and annihilated from the vacuum. Therefore as the Q^2 of the virtual photon increases it is able to probe smaller and smaller distances and so begins to resolve the particles within this cloud. Consequently we would expect the momentum distributions of the partons

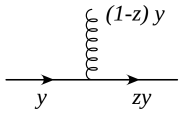

Figure 6: The quark-gluon vertex contributing to $P_{qq}(z)$

probed by the virtual photon to depend on Q^2 and it is this which leads to the violation of scaling mentioned earlier.

In order to study the form of this scaling violation - that is the peturbatively calculable dependence on the large scale Q^2 - we follow an approach originally due to Altarelli and Parisi [7] and consider the case where a quark carrying momentum fraction y of the proton radiates a gluon so reducing its momentum fraction to $x = zy$ with the remaining $(1-z)y$ being carried away by the gluon (fig. 6).

Now If the probability of the quark changing its momentum fraction by z is $\mathcal{P}_{q\to qg}(z)$ then we would expect

$$q^{NS}(x) = \int_0^1 \mathrm{d}y \int_0^1 \mathrm{d}z \; q^{NS}(y)\mathcal{P}_{q\to qg}(z)\delta(x - zy) \tag{25}$$

$$= \int_0^1 \frac{\mathrm{d}y}{y} q^{NS}(y)\mathcal{P}_{q\to qg}\left(\frac{x}{y}\right) \tag{26}$$

(where we have used the *non-singlet* quark distribution for a single flavour $q^{NS}(x) \equiv q(x) - \bar{q}(x)$)

In the QPM the momentum fraction of the quark before and after the hard scattering is constant so that $x = y$ and $z = 1$ and $\mathcal{P}_{q\to qg}(z) = \delta(1-z)$ and (26) is trivially satisfied for all Q^2 resulting in the observation of scaling. However, at $\mathcal{O}(\alpha_s)$, the quark can radiate gluons thus reducing its momentum fraction giving $y \geq x$. It is possible to calculate the probability of this from simple Compton scattering and we obtain

$$\mathcal{P}_{q\to qg}(z,t) = \delta(1-z) + \frac{\alpha_s}{2\pi}P_{qq}(z)t \tag{27}$$

where the *splitting function* $P_{qq}(z)$ is given in the leading log approximation - that is, keeping only the contribution which is most singular in the transverse momentum of the scattered quark and has the form

$$P_{qq}(z) \equiv \frac{4}{3}\left(\frac{1+z^2}{1-z}\right), \tag{28}$$

and we have defined $t = \ln Q^2/\mu^2$ where μ^2 is effectively some lower cut off required in order to regulate the infra-red divergence of the integration over the fermion propagator transverse momentum and is of the form,

$$\int_{\mu^2}^{Q^2} \frac{\mathrm{d}k_T^2}{k_T^2} P_{qq}(z). \tag{29}$$

Consequently we shall find that we need to redefine what we mean by our parton distributions and we eventually end up with the evolution equation

$$\frac{\partial}{\partial t} q^{NS}(x,t) = \frac{\alpha_s}{2\pi}\int_x^1 \frac{\mathrm{d}y}{y} q^{NS}(y,t) P_{qq}\left(\frac{x}{y}\right). \tag{30}$$

We see from (27) that we have two potential sources of singular behaviour. The first comes from the $(1-z)$ term in the splitting function as $z \to 1$. This corresponds to the limit of soft gluon emission, and is in fact cancelled against the infra-red singularities of the virtual 1 loop corrections to the $\gamma^* q \to q$ process ie. the vertex term of fig. 4c and the 1 loop corrections to the quark propagators. This cancellation occurs order by order in peturbation theory and is a consequence of the Kinoshita-Lee-Nauenberg [8] and Bloch-Nordsieck theorems [9].

It can be shown [10] that the cancellation of the infra-red singularities and the inclusion of properly dressed quark propagators leads only to the replacements

$$\alpha_s \to \alpha_s(Q^2) \tag{31}$$

and

$$P_{qq}(z) = \frac{4}{3}\left(\frac{1+z^2}{1-z}\right)_+ \equiv \frac{4}{3}\left[\frac{1+z^2}{(1-z)_+} + \frac{3}{2}\delta(1-z)\right] \tag{32}$$

where the "+" prescription is defined by

$$\begin{aligned}\int_x^1 \mathrm{d}z\, \frac{f(z)}{(1-z)_+} &\equiv \lim_{\delta\to 1} f(1)\ln(1-\delta) + \int_x^1 \mathrm{d}z\, \frac{f(z)}{1-z} &(33)\\ &= f(1)\ln(1-x) + \int_x^1 \mathrm{d}z\, \frac{f(z)-f(1)}{1-z} &(34)\end{aligned}$$

where we have subtracted the $\delta \to 1$ singularities. From (32) we see that

$$\int_0^1 \mathrm{d}z P_{qq}(z) = 0 \tag{35}$$

which means that taking (30) and integrating over x results in

$$\begin{aligned}\frac{\partial}{\partial t}\int_0^1 \mathrm{d}x\ q^{NS}(x,t) &= \frac{\alpha_s(t)}{2\pi}\int_0^1 \mathrm{d}x \int_x^1 \frac{\mathrm{d}y}{y} q^{NS}(y,t) P_{qq}\left(\frac{x}{y}\right) &(36)\\ &= \int_0^1 \mathrm{d}y\ q^{NS}(y,t)\int_0^1 \mathrm{d}z\ P_{qq}(z) &(37)\\ &= 0 &(38)\end{aligned}$$

which is just a statement of flavour conservation as we would expect.

Having now dealt with the soft divergences we are now left with the collinear divergence as $k_T^2 \to 0$ in the integration of (29). There are no more divergences to cancel this against so we must absorb this divergence into a redefinition of our quark distribution functions. How we choose to share factors between the splitting and distribution functions specifies our choice of *factorisation scheme* and effectively states at what value of transverse momentum we choose to factorise the cross section into hard (peturbative) and soft (non-peturbative) contributions. That we are able to do this, is of crucial importance for the calculation of observables using peturbative QCD.

To see how we do this we return to equation (18) inserting the form of the distribution functions (26);

$$\frac{F_2}{x} = \sum_q e_q^2 \int_x^1 \frac{\mathrm{d}y}{y} q(y)\left[\delta\left(1-\frac{x}{y}\right) + \frac{\alpha_s}{2\pi}P_{qq}\left(\frac{x}{y}\right)\ln\frac{Q^2}{\mu^2}\right] \tag{39}$$

(and we have neglected some renormalisation scheme dependent functions). However, the quantity on the left hand side contains a measurable quantity, ie.

the structure function, and so should be finite, so we somehow have to absorb the singular behaviour of the log term into our distribution functions, which - for this purpose - we consider to be effectively *bare* distribution functions which are themselves non-finite. To do this we factor off, from the $\mathcal{O}(\alpha_s)$ term a term or the form

$$\frac{\alpha_s}{2\pi} P_{qq}\left(\frac{x}{y}\right) \ln \frac{M^2}{\mu^2} \tag{40}$$

where M^2 is some arbitrary mass scale, and make the replacement of *renormalised* distribution functions

$$q(y) \to q(y, M^2) = q(y) + \frac{\alpha_s}{2\pi} K(y, M^2). \tag{41}$$

This is because we would like (39) to be – to $\mathcal{O}(\alpha_s)$– of the form

$$\frac{F_2}{x} = \sum_q e_q^2 \int_x^1 \frac{\mathrm{d}y}{y} q(y, M^2) \left[\delta\left(1 - \frac{x}{y}\right) + \frac{\alpha_s}{2\pi} P_{qq}\left(\frac{x}{y}\right) \ln \frac{Q^2}{M^2}\right] \tag{42}$$

such that the log term and the distribution functions themself are now finite. It is reasonably straight-forward to show that to $\mathcal{O}(\alpha_s)$ this is achieved by the replacement

$$K(y, M^2) = \int_y^1 \frac{\mathrm{d}y'}{y'} q(y', M^2) P_{qq}\left(\frac{y'}{y}\right) \ln \frac{M^2}{\mu^2}. \tag{43}$$

which, after iteratively substituting our renormalised distribution functions, gives us, to $\mathcal{O}(\alpha_s)$, the form of the evolution equation (30) which shows how they evolve with the scale M^2 and now all our distributions are finite. This procedure is known as *mass factorization.*

It is straightforward to generalise the evolution equation for the flavour non-singlet distribution functions (30) to the flavour singlet case by the inclusion of the gluon density $G(x,t)$. This allows for the possibility of a gluon producing either a $q\bar{q}$ or a gg pair. Taking account of flavour conservation and assuming flavour universality of the quark-gluon vertex we obtain the so-called *Altarelli-Parisi* evolution equations (or more correctly the Dokshitzer-Gribov-Lipatov-Altarelli-Parisi evolution equations) [7, 10]

$$\frac{\partial}{\partial t} q^i(x,t) = \frac{\alpha_s(t)}{2\pi} \int_x^1 \frac{\mathrm{d}y}{y} \left[P_{qq}\left(\frac{x}{y}\right) q^i(y,t) + P_{qG}\left(\frac{x}{y}\right) G(y,t)\right] \tag{44}$$

$$\frac{\partial}{\partial t} G(x,t) = \frac{\alpha_s(t)}{2\pi} \int_x^1 \frac{\mathrm{d}y}{y} \left[\sum_i^{2N_f} P_{Gq}\left(\frac{x}{y}\right) q^i(y,t) + P_{GG}\left(\frac{x}{y}\right) G(y,t)\right] \tag{45}$$

where we have summed over both quarks and anti-quarks in the first term of (45) and where $P_{Gq}(z)$, $P_{qG}(z)$ and $P_{GG}(z)$ are the splitting functions for obtaining a gluon from a quark, a quark from a gluon and a gluon from a gluon respectively and are given by

$$P_{qG}(z) = \frac{N_f}{2}\left[z^2 + (1-z)^2\right] \tag{46}$$

$$P_{Gq}(z) = \frac{4}{3}\left[\frac{1 + (1-z)^2}{z}\right] \tag{47}$$

$$P_{GG}(z) = 6\left[\frac{z}{(1-z)_+} + \frac{1-z}{z} + z(1-z) + \left(\frac{11}{12} - \frac{N_f}{18}\right)\delta(1-z)\right]. \tag{48}$$

If we now form the combination $q^S(x,t) \equiv \sum_i^{2Nf} q^i(x,t)$, again summing over quarks and anti-quarks of all flavours then equations (44) and (45) take the form

$$\frac{\partial}{\partial t}\begin{bmatrix} q^S(x,t) \\ G(x,t) \end{bmatrix} = \frac{\alpha_s(t)}{2\pi} \int_x^1 \frac{\mathrm{d}y}{y} \begin{bmatrix} P_{qq} & 2N_f P_{qG} \\ P_{Gq} & P_{GG} \end{bmatrix} \begin{bmatrix} q^S(y,t) \\ G(y,t) \end{bmatrix}. \tag{49}$$

In general any parton distribution can be decomposed into singlet and non-singlet contributions each evolving with Q^2 according to (49) or (30) respectively.

If we now define the moments $M^n(t)$ of the distribution function $q(x,t)$ by the Mellin transform

$$M_n(t) = \int_0^1 \mathrm{d}x \; x^{n-1} q(x,t) \tag{50}$$

then this enables us to seperate the integrals[3]

$$\frac{\partial}{\partial t}\begin{bmatrix} M_n^S(t) \\ M_n^G(t) \end{bmatrix} = \frac{\alpha_s(t)}{2\pi} \begin{bmatrix} P_{qq}^n & 2N_f P_{qG}^n \\ P_{Gq}^n & P_{GG}^n \end{bmatrix} \begin{bmatrix} M_n^S(t) \\ M_n^G(t) \end{bmatrix}. \tag{51}$$

the solution of which can be found by diagonalising.

These equations, although specifying exactly how the distributions evolve with Q^2 (provided we know their form at some additional scale Q_0^2), do not fully determine the form of the distributions themselves which are of course highly non-peturbative. As such these have to be obtained using parameterisations of experimental data. See, for example [11, 16, 15] for some recent parameterisations.

[3] where P_{qq}^n is the nth moment of $P_{qq}(z)$ etc.

2.1.1 Summing the Leading Logs

Further insight can be gleaned by reconsidering the $\mathcal{O}(\alpha_s)$ contribution to the process $\gamma^* q \to qg$ in DIS. These are shown in fig. 4(a) and 4(b) which represent gluon emission from the initial and final state quark propagators respectively and give rise in the Leading Log approximation, to a contribution is of the form

$$\alpha_s(Q^2) P_{qq}(z) \ln \frac{Q^2}{\mu^2} \tag{52}$$

where we have included the running of the coupling constant. From (24) we see that the factor $\alpha_s(Q^2)\ln Q^2/\mu^2$ is of order 1 and so has the ability to spoil our peturbative expansion. Therefore we must re-sum all contributions of the form $[\alpha_s(Q^2)\ln Q^2/\mu^2]^n$ to ensure our result is finite. This means we must sum all diagrams with $N = 1, \ldots, \infty$ gluons. An example of an initial state n gluon diagram is fig. 7.

These correspond to a particular subset of the complete expansion in α_s to all orders.

We would like to be able to calculate this as a summation of terms such that each is merely of the form of the term for emission of one gluon to some power.

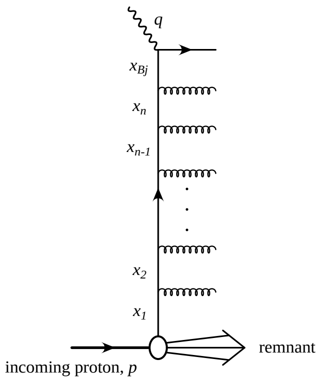

Figure 7: N gluon emission in the initial state

This scenario is called *independent emission*. However this is not possible because of the interference terms. We illuminate this by considering the calculation of the emission of 1 gluon from the flavour non-singlet state.

If we consider only the *inclusive* reaction and are not interested in the details of the final state, then we effectively sum over the complete set of final states and need only consider the elastic scattering amplitude. This is known as the *optical theorem* and means that we can calculate the matrix elements for the $\mathcal{O}(\alpha_s)$ $\gamma^* q \to qg$ processes using the diagrams of fig. 8.

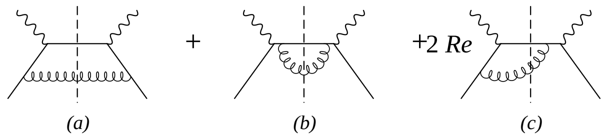

Figure 8: The $\mathcal{O}(\alpha_s)$ contribution to the process $\gamma^* q \to qg$

Individually, the contributions from these diagrams are not gauge invariant, only their overall sum, and as our final calculation must be independent of the gauge in which we evaluate, we are free to chose any gauge and find that we are able to move contributions around between diagrams. If we chose an axial gauge where the sum over gluon spin states is given by

$$\sum_\lambda \varepsilon^\mu(\lambda)\varepsilon^\nu(\lambda) = -g^{\mu\nu} + \frac{n^\mu k^\nu + n^\nu k^\mu}{n.k} - \frac{n^2}{(n.k)^2} k^\mu k^\nu \tag{53}$$

where n^μ is an arbitrary 4-vector satisfying $\varepsilon.n = 0$ (and usually also $n^2 = 0$) it is found that we need only consider the diagram 8a as the diagram 8b and the interference diagram 8c do not contribute. Here the collinear divergence or the gluon radiation is cancelled by the infra-red divergence of the virtual terms, however the divergence of the initial state radiation has an extra contribution which we deal with by absorbing into the parton distribution as explained earlier.

This means that - provided we work in an axial gauge - we need only consider ladder diagrams of the form of figure 9 where we have *independent emission.*

In this diagram, the quark propagator from each cell carries a momentum fraction x_i and a squared transverse momentum k_{Ti}^2 (as indicated in fig. 9). Conservation of energy gives us the condition that

$$x_1 > x_2 > \cdots > x_N > x_{Bj} \tag{54}$$

and the dominant contribution comes from the region of phase space where

$$k_{T1}^2 \ll k_{T2}^2 \ll \cdots \ll k_{TN}^2 \ll Q^2. \tag{55}$$

As such for N gluon emission we obtain a nested integral of the form

$$q_{(N)}^{NS}(x,t) \sim \frac{1}{N!}\xi^N(t)\int_x^1 \frac{\mathrm{d}x_N}{x_N}P_{qq}\left(\frac{x}{x_N}\right)\int_{x_N}^1 \frac{\mathrm{d}x_{N-1}}{x_{N-1}}P_{qq}\left(\frac{x_N}{x_{N-1}}\right)\cdots \int_{x_2}^1 \frac{\mathrm{d}x_1}{x_1}P_{qq}\left(\frac{x_2}{x_1}\right)q^{NS}(x_1,t_c) \qquad (56)$$

where the term $\xi^N(t)$ comes from the integration over the quark transverse momenta,

$$\frac{1}{N!}\xi^N(t) \equiv \frac{1}{N!}\left[\frac{\ln t}{b_0}\right]^N = \int_{t_c}^{t}\frac{\mathrm{d}t_1}{b_0t_1}\int_{t_c}^{t_1}\frac{\mathrm{d}t_2}{b_0t_2}\cdots\int_{t_c}^{t_{N-2}}\frac{\mathrm{d}t_{N-1}}{b_0t_{N-1}}\int_{t_c}^{t_{N-1}}\frac{\mathrm{d}t_N}{b_0t_N} \qquad (57)$$

where t_c is our lower cutoff in transverse momentum and $t = \ln Q^2/\Lambda^2$ such that to leading order $\alpha_s(t) = 1/b_0t$ - hence the $1/b_0t$ terms in the integrations. Here we note that the use of the arbitrary lower cutoff t_c merely states at which point along the ladder we choose to factorize the calculation into soft and hard contributions.

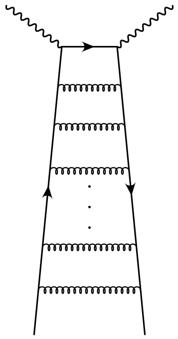

Figure 9: Parton ladder contribution in the leading log approximation

Our final parton distribution is then obtained by summing all diagrams with $N = 1\ldots\infty$ gluons ie;

$$q^{NS}(x,t) = \sum_{N=0}^{\infty} q^{NS(N)}(x,t). \qquad (58)$$

If we first take the Mellin moments $M_n^{NS}(t)$ of $q^{NS}(x,t)$ and (56) this gives us the following expression for the N rung diagram

$$M_{n(N)}(t) = \frac{1}{N!}\xi^N(t)\left[\int_0^1 \mathrm{d}z\ z^{n-1}P_{qq}(z)\right]^N\left[\int_0^1 \mathrm{d}y\ y^{n-1}q(y,t_c)\right] \qquad (59)$$

$$\equiv \frac{1}{N!}\xi^N(t)[P_{qq}^n]^N M_n(t_c) \qquad (60)$$

which upon performing the summation gives

$$M_n(t) = \exp\left[\xi(t)P_{qq}^n\right]M_n(t_c). \qquad (61)$$

which we differentiate to produce

$$\frac{\partial M_n(t)}{\partial t} = \alpha_s(t)P_{qq}^n M_n(t). \qquad (62)$$

This is just the form of (30) in moment space, and so we have obtained our parton distribution evolution equation by explicitly summing over all N rung ladder diagrams of the form fig. 9. It is possible to generalise this approach to include colour singlets if we also consider the contributions from gluon cells and the triple gluon vertex, shown right.

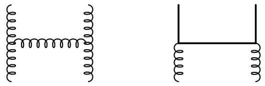

Their inclusion then allows for mixing between the various integral kernels - of which the flavour non-singlet is only one. From this we are then able to obtain the moment space DGLAP equations (51) in a similar manner, the solutions of which can be obtained by diagonalising as mentioned.

3 Peturbative QCD at small x

3.1 The Double Leading Log Approximation

Because the DGLAP equations are derived keeping only the leading log terms in Q^2, terms of the form $\ln(1/x)$ are neglected unless accompanied by a large log in Q^2. At normal values of x this is acceptable as these terms are small, however as $x \to 0$ these obviously become important.

Consequently, at small x we should sum all $\ln(1/x)$ terms in our peturbative expansion, however some mileage may still be found in the DGLAP equations in the small x region provided we also take Q^2 as large. This means that keep only terms containing large logarithms of both $1/x$ *and* Q^2. This is the so-called *Double Leading Log Approximation* (DLLA).

In the DLLA we continue to use the A-P splitting functions, which in the limit $z \to 0$ become

$$P_{qq}(z) \to \frac{4}{3}, \qquad P_{qG}(z) \to \frac{N_f}{2} \tag{63}$$

$$P_{Gq}(z) \to \frac{2}{z}, \qquad P_{GG}(z) \to 6\frac{1}{z}. \tag{64}$$

From these we see that at small x the leading contribution will come from the *gluon distribution*, which means that in physical gauges the dominant contribution will be from ladder diagrams with *only* gluons present. This is what we would expect intuitively as the valence quark distributions are expected to vanish as $z \to 0$ and the sea quarks are expected to be driven by the gluon distribution via $q\bar{q}$ production.

In the DLLA the strong ordering in k_T still remains, however the usual ordering of the longitudinal momentum fractions x_i also become strong. That is

$$1 \gg x_1 \gg \ldots \gg x_N \gg x. \tag{65}$$

The evolution equation for the gluon momentum distribution $xG(x,t)$ then takes the form

$$\frac{\partial xG(x,t)}{\partial \ln t} = \frac{6\alpha_s(t)}{2\pi} \int_0^{\ln\frac{1}{x}} \mathrm{d}\left(\ln\frac{1}{y}\right) yG(y,t) \tag{66}$$

from which we obtain

$$\frac{\partial^2 xG(x,t)}{\partial \ln t \; \partial \ln(1/x)} = \frac{1}{2} K xG(x,t) \tag{67}$$

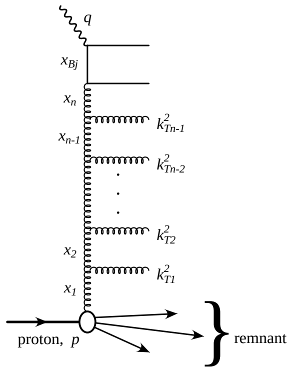

Figure 10: n rung ($n-1$ gluon) emission in the DLLA

where $K = 6/\pi b_0$. This has the solution in the limit where $xG(x,t) \gg 1$

$$xG(x,t) \sim \exp\left[2K \ln t \ln\frac{1}{x}\right]^{\frac{1}{2}} \tag{68}$$

and again, we have included the running of the coupling constant.

Therefore in the small x limit we would expect from (68) a gluon distribution that rises faster than any single power of $\ln(1/x)$ yet slower than any (negative) power of x.

This should therefore be the dominant contribution to the proton structure function in the region where both $\ln(1/x) \gg 1$ and $\ln Q^2 \gg 1$.

3.2 The Leading Log $(1/x)$ Approximation

The DLLA is of course not valid in the region of finite Q^2, where we must re-sum all the $\ln(1/x)$ terms, not just those accompanied by a large log in Q^2.

This summation is known as the leading log $(1/x)$ approximation (LL$(1/x)A$) and results in the the Lipatov (or more correctly the *Balitskii-Fadin-Kuraev-Lipatov* - BFKL) equation [12].

In order to obtain the LL$(1/x)$A our soft ordering of the longitudinal momentum fraction becomes strong (as in the DDLA) and it is necessary to drop the strong ordering in transverse momentum and integrate over the complete phase space.

Consequently - in an axial gauge - besides the contribution from ladder diagrams resulting from gluon emission as in fig. 10 there is also a contribution from non-ladder diagrams which include virtual corrections.

As a result, the form of the resummation is presently derived only for a fixed α_s - although it may be of some use phenomenologically to use a running coupling. In our previous discussion of the LLA and DLLA we used a running coupling, however the approximation to a fixed coupling is reasonably trivial, and will not be dwelt upon.

In this case, both the DLLA and the BFKL evolution with both x and Q^2 can be written in the form

$$f(x,k_T^2) = f^{(0)}(x,k_T^2) + \int_0^\infty \frac{\mathrm{d}k_T'^2}{k_T'^2} K(k_T,k_T') \int_x^1 \frac{\mathrm{d}y}{y} f(y,k_T'^2) \tag{69}$$

where the $f(x,k_T^2)$ is related to the *un-integrated* gluon distribution given by

$$xG(x,Q^2) = \int_0^{Q^2} \frac{\mathrm{d}k^2}{k^2} f(x,k^2), \tag{70}$$

and as before we expect the dominant contribution to be due to that of the gluon. The strong ordering of the DLLA means that the integral kernel $K(k_T,k_T')$ simply reduces to the form

$$K(k_T,k_T') = \frac{3\alpha_s}{\pi}\frac{1}{k_T^2}\theta(k_T^2 - k_T'^2) \tag{71}$$

so that the integral over the θ function just reproduces the standard integration over the *ordered* transverse momentum.

The Lipatov kernel however (which sums the more complicated, non-ladder diagrams which we ignore in the LL(Q^2) DGLAP approximation) takes the more complicated form

$$K(k,k') = \frac{3\alpha_s}{\pi}k^2 \left[\frac{1}{k'^2\,|k'^2-k^2|} - \beta(k^2)\delta(k^2-k'^2)\right] \tag{72}$$

where we are using $k^2 \equiv k_T^2$ and the function β is given by

$$\beta(k^2) = \int \frac{\mathrm{d}k'^2}{k'^2}\left[\frac{1}{|k'^2-k^2|} - \frac{1}{[4k'^4+k^4]^{\frac{1}{2}}}\right]. \tag{73}$$

The singularity at $k'^2 = k^2$ apparently cancels between the real and virtual contributions and the resulting kernel is infra-red safe.

Inserting (72) into (69) results in

$$x\frac{\partial f(x,k^2)}{\partial x} = \frac{3\alpha_s(k^2)}{\pi}k^2\int_0^\infty \frac{\mathrm{d}k'^2}{k'^2}\left[\frac{f(x,k'^2)-f(x,k^2)}{|k'^2-k^2|} + \frac{f(x,k^2)}{[4k'^4+k^4]^{\frac{1}{2}}}\right] \tag{74}$$

if we assume that the inhomogeneous $f^{(0)}(x,k_T^2)$ term which represents the (non-peturbative) gluon-proton coupling is flat for small x [13] ie $f^{(0)}(x,k_T^2) \approx f(x_0,k_T^2)$ for sufficiently small $x_0 \geq x$.

Equation 74 has been solved analytically for asymptotically small x [14] and results in the behaviour

$$f(x,k^2) \sim x^{-\lambda}\left[\frac{k^2}{\ln(1/x)}\right]^{1/2}\exp\left[\frac{-\ln(k^2/k_0^2)}{\Delta\lambda\ln(1/x)}\right], \tag{75}$$

where λ is the leading eigenvalue of the kernel K;

$$\lambda = \frac{3\alpha_s}{\pi}4\ln 2, \tag{76}$$

and Δ and k_0 determine the width and the centre of the k_T distribution which is no longer strongly ordered instead following a "random walk" along the gluon ladder. This means that for $\alpha_s \approx 0.2$ we expect $f \sim x^{-\lambda}$ where $\lambda \approx \frac{1}{2}$.

Recent measurements of the structure function $F_2(x,Q^2)$ from HERA [24] demonstrate clearly a rise at low x entirely consistent with the $x^{-\lambda}$ behaviour of the BFKL prediction. However, due to the inclusive nature of $F_2(x,Q^2)$ the observed small x behaviour can also be explained by traditional DGLAP evolution, starting from a very small scale $Q^2 = 0.3\mathrm{GeV}^2$ [15].

Consequently, current measurements of $F_2(x,Q^2)$ do not seem incisive enough to distinguish between BFKL and conventional DGLAP dynamics and so in an attempt to do so we must examine the properties of the hadronic final state.

4 The Hadronic Final State

Because we are interested in the properties of the hadronic final state, it is not sufficient that we consider only ladder diagrams as before, we must include the entire final state. This means we need to allow for the case of interfering gluons, and also the effects of non-peturbative, long-range confinement effects which describe how the partons in the final state become confined inside the observed hadrons.

In section 1 it was mentioned that the partonic constituents of the hadrons were permanently confined within them, however, that at large momentum transfers, their dynamics were such that they behaved as effectivly free. Consequently, when describing a typical DIS event we "factorize" the behaviour of the final state system into the peturbative hard scattering and the non-peturbative, fragmentation or hadronization. In between these two processes we have the development of the time-like parton showers whereby the highly virtual partons, undergo peturbative QCD radiation to produce a final state of many partons with smaller invariant mass. It is these that undergo the process of fragmentation, with the parton virtuality acting as the factorization scale specifying how we separate the peturbative and non-peturbative regimes.

However, the non-peturbative nature of fragmentation means that we do not have a clear understanding of just how this takes place, and so as in the case of the structure function input at small scales, we are forced to use phenomenological models which parameterise our ignorance of the exact mechanism.

This factorization property allows us to simulate the overall evolution of the final state in the form of a Monte Carlo. In this approach we allow for the development of both initial and final state parton showers separately from the hard scattering, down till some parton virtuality cutoff, after which the hadronisation mechanism is invoked to produce the final state hadrons. These are then allowed to either decay or interact in the detector accordingly.

4.1 The Parton Shower

4.1.1 The Matrix Element-Parton Shower Approach

The parton shower is usually treated using traditional DGLAP evolution although taking account of interfering gluons. This is often known as the Matrix Element-

Parton Shower (MEPS) approach, as implemented in LEPTO [28] which includes the $\mathcal{O}(\alpha_s)$ matrix elements and a LL parton shower for the final state and initial state gluon emission in the central region. Consequently, in the low x region, we would simplistically expect the k_T^2 ordering of the initial state DGLAP parton shower to produce a lower transverse energy in the forward region than that predicted from BFKL evolution, due to the increased phase space available for the initial state "gluon" radiation in the BFKL scenario.

4.1.2 The Colour Dipole Model

Besides the MEPS model there is an additional model for the generation of the parton shower known as the Colour Dipole Model (CDM) [31] as implemented in ARIADNE [32]. This treats pairs of partons in the final state (ie. the proton remnant diquark, struck quark etc.) as a series of (increasingly numerous) colour dipoles which are free to radiate gluons. In this model, the strong k_T^2 ordering of the DGLAP evolution is relaxed and consequently we expect a slightly higher value for the transverse energy in the forward region at low x. Because of the relaxation of the strong ordering it may be the case that the CDM simulates some of the features of the BFKL evolution, although this is by no means clear at the moment.

Despite the apparent success of the CDM in explaining some of the features of the forward energy flows [38, 39], it should be noted that CDM has no mechanism for generating the leading order interaction of the gluon with the virtual photon, and consequently, the boson-gluon fusion matrix element has to be included separately to generate the initial system of radiating dipoles. This is known as the CDM+BGF scenario.

4.2 Hadronisation

There are several models of the hadronisation process which are implemented in the Monte Carlos. Two of the most used are Lund String Fragmentation [34] as implemented in JETSET and Cluster Fragmentation [35] as implemented in HERWIG.

4.2.1 The Lund String Model

In this model, outgoing quarks being in a colour triplet state are considered to be connected by *strings* (ie. a colour flux tubes) stretched between them. At small separations, the asymptotic freedom of the strong interaction means that they are considered as essentially free, although connected. However as they move apart the string becomes "stretched", increasing the string tension until there is sufficient energy for $q\bar{q}$ pairs to be produced from the vacuum, enabling the string to split. This process continues with the strings fragmenting into smaller and smaller pieces and creating more parton-antiparton pairs until the energy of the partons is insufficient to cause any further splitting. As a result we obtain a system made of many small colour singlet clusters of partons which are then able to form the observed hadrons. The actual process of the string fragmentation is governed by a *string fragmentation function* which parameterises the properties of the splitting of the string such as the amount and distribution of transverse momentum of the clusters and so on.

The topology of the strings is modified by the presence of gluons which cause "kinks" and so in turn modify the 4-momenta of the string fragments and so the momentum distribution of the final state hadrons.

4.2.2 The Cluster Fragmentation Model

In the cluster fragmentation model [35], after the generation of the peturbative parton shower, any gluons in the parton final state are forcibly split into $q\bar{q}$ pairs. This results in a system of quarks and anti-quarks with a colour topology where each quark is connected to an anti-quark with which it forms a colour singlet "cluster". These clusters are then allowed to decay isotropically to hadrons by a simple two body decay, unless there is insufficient energy to create two hadrons, in which case the cluster is considered to represent the lightest hadron of its flavour with the cluster mass being adjusted by momentum transfer with adjacent clusters.

Where the mass of the cluster is too high for isotropic dacay to be considered reasonable, ie above some *fission threshold* then a series of subsequent decays are allowed until all the fragments are below this threshold, and in this respect is not entirely dis-similar to the string fragmentation model.

5 The Transverse Energy Flow

One such measure is the so called *Energy Flow* $\frac{1}{N}\frac{\mathrm{d}E}{\mathrm{d}\Omega}$ which measures the distribution of hadronic energy into a region of solid angle $\mathrm{d}\Omega$ and is normalised to the total number of events N in our data sample. In practice however, as the colliding system is azimuthally symmetric about the beam direction, we chose to integrate over the azimuthal angle giving us the differential energy flow into an interval of pseudo-rapidity $\mathrm{d}\eta$ (where $\eta = -\ln\tan\theta/2$). Experimentally at HERA, because of the large longitudinal boost along the proton beam direction we consider the transverse component of the energy flow E_T,

$$\frac{1}{N}\frac{\mathrm{d}E_T}{\mathrm{d}\eta} = \frac{1}{N}\sum_{n=1}^{N}\left[\frac{\mathrm{d}E\sin\theta}{\mathrm{d}\eta}\right]_n \qquad (77)$$

where the summation is over the N events in our data sample and the differential energy flow in the bracket is the generic flow for each individual event (that is, the summation over all the hadrons in the final state, calorimeter cells, etc.).

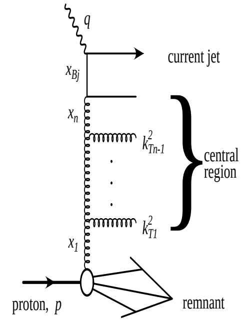

Figure 11: The low x final state in neutral current DIS

In the QPM the struck quark scatters to some angle γ_h as mentioned earlier and the proton remnant (consisting of a diquark in the case of scattering off a valence quark) continues along the proton beam direction. In practice, [4] the developement of the parton shower and the subsequent hadronisation of the partonic system results in the formation of collimated *jets* of hadrons in the final state approximately along the direction of the struck quark (the *current jet*) and the direction of the proton remnant. Additionally, the region between the proton remnant and the current - the so-called *central region* - is also populated with hadronic material.

However, at the parton level, at low x, we also must consider the emission of QCD radiation from the initial state in order to perform the leading log resummation and we expect that this also adds to the level of hadronic material in the central region. This is illustrated in figure 11.

5.1 Theoretical Prediction for the Low x Transverse Energy Flow

Consequently, when calculating the non-trivial contribution to the transverse energy in the central region to leading order we consider the single particle inclusive cross-section weighted by the transverse energy. As in the case of the parton distribution functions at low x we again consider the dominant contribution to come from the gluon, and so consider diagrams with one observed parton in the final state, and we resum the gluon ladders both above and below the emitted parton. This calculation has been performed by Golec-Biernat *et al.*[25]. Their calculation uses a BFKL approach to resum the large $\ln(1/x)$ contributions, both analytically for a fixed α_s and numerically with a running coupling.

This demonstrates that the relaxation of the strong k_T^2 ordering for the BFKL calculation does indeed lead to a strong enhancement of the transvere energy compared to that using traditional k_T^2 ordered Alteralli-Parisi dynamics and further that the energy flow as a function of rapidity is expected to show a $\sim x^{-\epsilon}$ dependence rising with small x whereas a DGLAP calculation is expected to fall with decreasing x.

5.1.1 Problems with the BFKL Equation

Despite the apparent success of BFKL dynamics at the parton level at least, problems do remain, notably the fact that the k_T^2 integrations extend down into

[4] neglecting so-called *rapidity gap events* for the moment

the infra-red region. This suggests problems accepting the finite order peturbation theory of the BFKL equation. This can be partly overcome for example by the use of higher order corrections which effectively means the replacement of the fixed α_s with a running coupling. This modification however - in altering the low energy behaviour - loses the infra-red finiteness of the BFKL kernel and requires the use of an infra-red cutoff. Other methods have also been used, and ultimately, any calculations must be demonstrated to be insensitive to the treatment of the infra-red limit [18, 19].

Additionally the upper limit in the integrations leads to energy non-conservation and so the calculations should also be expected to be insensitive to any ultra-violet behaviour [20]. The imposition of Energy conservation makes the calculations considerably more difficult, and may lead to a slower growth of the gluon distribution at small x [20].

Precisely how these problems are to be overcome and what their overall effect will be is at present not well understood and so present problems with unabiguously determining the form of the peturbative QCD predictions in the low x region in DIS.

It should be noted that thess calculations do not include any contribution for the effects of hadronization, nor for the presence of time-like showering from the final state partons including the current jet. Consequently, in order to more properly test the details of BFKL dymanics in this region, a BFKL inspired Monte Carlo would be required. At the time of writing no such Monte Carlo exists, however, one is under construction by Golec-Biernat and may be available soon.

6 Results From Monte-Carlo Simulation

6.1 The New Monte Carlos

6.1.1 HERWIG 5.8d

For the analysis of the 1993 H1 data [39] the H1 collaboration used HERWIG 5.7 with a combination of their own tuning for some of the HERWIG parameters, the MRSD-' [27] structure functions and the inclusion of a *soft underlying event* (SUE). The SUE is a simulation of a "soft" collision between the proton remnant and the outgoing struck quark system superposed upon the hard scatter and was required to give the event the required energy in the forward region. Since then an updated version - HERWIG 5.8 - has been released, although this does not significantly modify the observed energy flow [42]. The new version however (HERWIG 5.8d [37]) has, among other changes, a modified treatment of the proton remnant, whereby the remnant cluster is allowed to decay asymmetrically. As a consequence of this modification, the use of the soft underlying event is now no longer recommended.

6.1.2 ARIADNE 4.07

The new version of the ARIADNE has a new default set of parameter tunings and also, like the new version of HERWIG a modified remnant treatment, which involves a modification to the treatment of the transverse extent of the remnant which in turn affects the generation of the the dipole cascade.

6.1.3 LEPTO 6.3

The new version of LEPTO [29] also has a modified treatment of the remnant, notably that of the sea quarks within the proton. This effectively increases the transverse energy in the forward region, however there is also the introduction of so called "soft colour interactions" (SCI) whereby the colour topology of the parton final state is modified by soft gluon exchange between the remnant and the struck quark system as it moves through the remnant's colour field. The purpose of this was initially to provide a mechanism for generating rapidity gap events within LEPTO (which up till version 6.3 included no mechanism for their generation). As the modification of final state parton colour topology naturally

allows the struck quark system to be in a colour singlet state so the strings for the struck quark and remnant systems need not be connected and are free to fragment independently so giving rise to the presence of gap events. The relative proportion of gap to non-gap events due to this rearrangement is controlled by a new parameter, which has been tuned for the default version of 6.3 [30]. The modification of the colour topology, affecting the arrangement of Lund string system also affects the fragmentation in non-gap events. This leads to the additional effect of an increase in the forward energy flow.

6.2 Comparison with H1 1992 data

For the analysis of the H1 1992 data [39] the H1 collaboration present data for the transverse energy flow, after unfolding for detector effects, corresponding to the physics cuts;

- E_e (energy of the scattered electron) > 14GeV.
- W^2 (Invariant mass of the hadronic system) > 3000 GeV^2.
- θ_e (the angle of the scattered electron) in the range $157.0° < \theta_e < 172.5°$.
- E_F (energy in the forward region $3.5° < \theta < 15°$) > 0.5 GeV.

This last cut is designed to remove most of the diffractive component. The data was binned in x into two bins $x > 10^{-3}$ and $x < 10^{-3}$.

6.2.1 HERWIG

Figures 12 and 13 show the comparison of HERWIG 5.8 and 5.8d with the data for the two x bins. In figure 12 we see the results of using the defaults settings of HERWIG 5.8 (solid line) the H1 tunings+SUE (dashed) and the defaults settings + SUE (dotted line). All histograms were generated with the MRSD-' structure functions, and show that without the soft underlying event HERWIG 5.8 is unable to generate sufficient energy in the forward region, particularly in the lowest x bin.

The use of the default tunings in conjunction with the SUE do appear to generate a slightly higher E_T than the use of the SUE with the H1 tuning, however this effect appears less significant than the addition of the SUE itself.

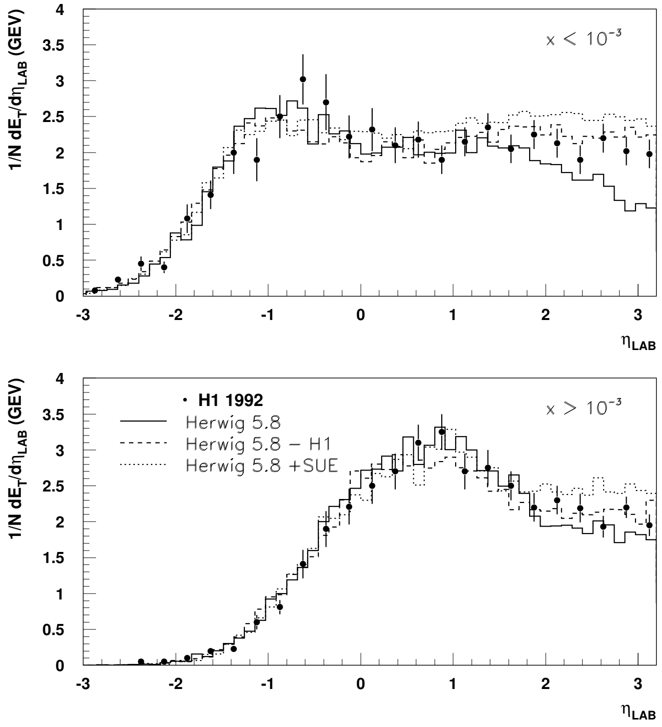

Figure 12: Transverse energy flows in the lab frame for H1 1992 data compared to HERWIG 5.8. (generated using the MRSD-'structure functions)

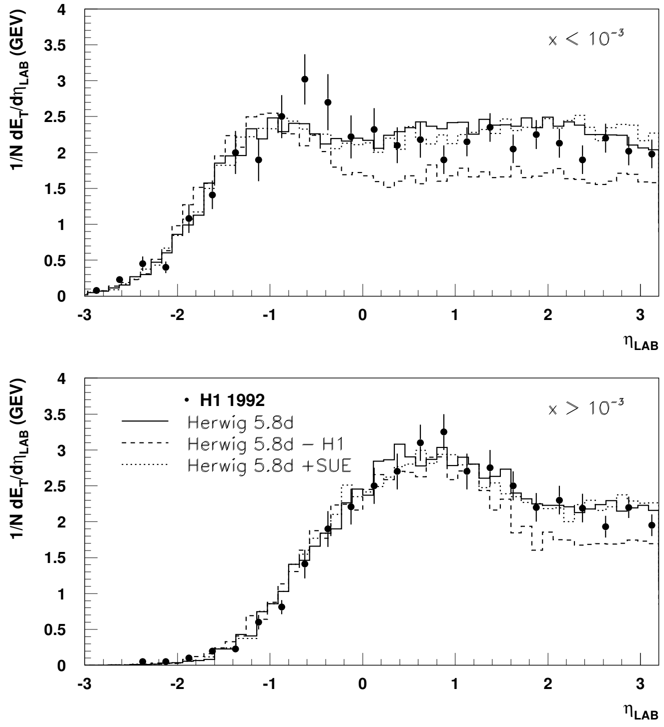

Figure 13: Transverse energy flows in the lab frame for H1 1993 data compared to HERWIG 5.8d. (MRSD-' structure functions)

In contrast (fig. 13), HERWIG 5.8d now appears to be able to describe the level of the energy flow, in both the higher and lower x bins without the need for a soft underlying event. In fact the addition of the SUE appears to cause only a slight modification in the energy flow, which should be contrasted to the use of the H1 parameter tunings, which appear to cause a significantly lower value for the energy flow in the forward region in both x bins.

6.2.2 ARIADNE and LEPTO

In figure 14 we see a comparison of the new version ARIADNE 4.07 (solid), LEPTO 6.1 (dashed) and LEPTO 6.3 (dotted), all with the default parameters. Form this figure we see that ARIADNE is still able to provide a reasonable description of the data. Also the new version of LEPTO is also seen to do well, whereas LEPTO 6.1 - the so called MEPS model - is seen to have too little energy in the forward region, and a current jet distribution which is too hard.

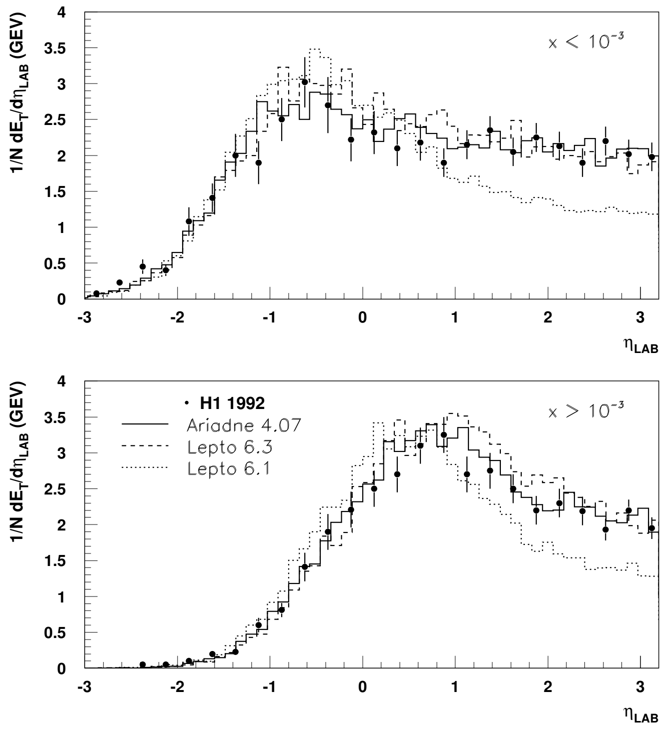

Figure 14: Transverse energy flows in the lab frame for H1 1993 data compared to ARIADNE and LEPTO

6.3 Comparison with ZEUS 1993 Data

The ZEUS collaboration present analysis of the 1993 ZEUS data [38] corresponding to the physics cuts;

- $Q^2 > 10$ GeV^2
- $x < 10^{-3}$
- $y < 0.95$
- $\eta_{\rm max} > 1.5$ where $\eta_{\rm max}$ is defined as the pseudo rapidity in the ZEUS frame of the particle/cluster closest to the "beam-pipe" with energy$>$ 0.4 GeV.

Again, this last cut is designed to remove so called rapidity gap events.

Figure 15 shows the results of the generator level simulation for all three Monte Carlos, with the same convention for the HERWIG parameter settings as with the H1 92 comparisons.

From this plot it is again clear that LEPTO 6.1 provides too little transverse energy flow in the forward region, whereas both ARIADNE and LEPTO 6.3 are consistent with the data - even though LEPTO 6.3 appears slightly lower than ARIADNE in the very far forward region, particularly in the region beyond the geometrical acceptance of the detector ($\eta > 4.3$).

Again, the default HERWIG 5.8 is unable to provide enough energy without the soft underlying event, whereas with the SUE the H1 tunings provide a better fit to the data, the default parameters again providing results which are too high. HERWIG 5.8d is again able to do well with the default parameters, with the use of the SUE increasing the energy flow only slightly in the very far forward region. Again with the H1 parameters, the E_T flow is systematically low.

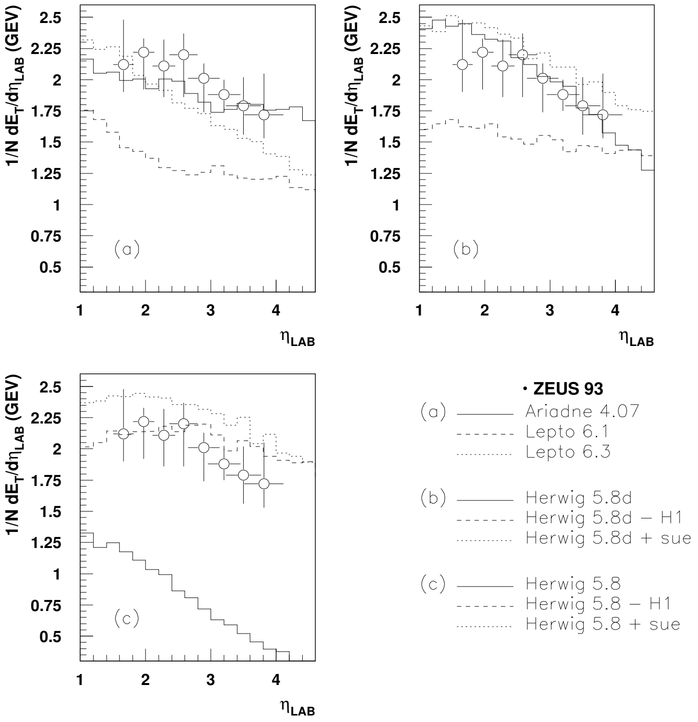

Figure 15: Transverse energy flows in the lab frame for ZEUS 93 data [38] compared to HERWIG ARIADNE and LEPTO

6.4 Comparison with the H1 1993 Data

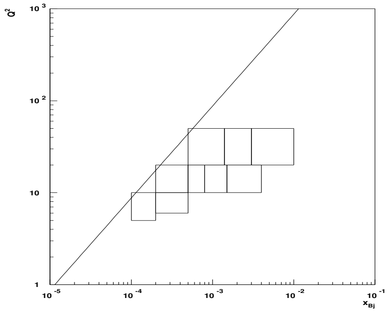

Figure 16: Kinematic bins for the H1 1993 Transverse Energy Flow Analysis [41].

With the increased statistics of the 1993 running, the H1 collaboration were able to subdivide the kinematic region up into 8 bins in x and Q^2 [41]. These bins are shown in figure 16. In addition to these kinematic cuts the data were unfolded to correspond to the physics cuts;

- $W^2 > 4400\mathrm{GeV}^2$.
- E_e >12GeV.
- $157^\circ < \theta_e < 173^\circ$
- $E_F > 0.5$ GeV.

6.4.1 HERWIG

Figures 17 and 18 show the generator level simulations for HERWIG 5.8 and 5.8d respectively. As before all histograms were generated using the MRSD-' structure functions and again follow the same convention in that the solid line is for the default parameters, dashed for the H1 tunings and dotted for the default tunings with the SUE.

As before we see that in the very low x and Q^2 bins the default HERWIG 5.8 is again unable to provide sufficient energy in the forward region, and additionally the current region also appears too soft wheras with the SUE, both with and without the H1 tunings the forward region in the low x bins ($< 10^{-3}$) appears reasonably well described (although in the very lowest x bin again the current region appears too soft). However at higher values of Q^2 the current region appears more adequately described with the default parameters and further that at the larger x values the use of the soft underlying event seems to provide too much energy in the forward region.

The default HERWIG 5.8d on the other hand, seems to provide an adequate description of the forward region at low x both with and without the SUE although again the current region does not appear well treated. At higher x and Q^2 the current region seems well described although the central region may be too peaked. Again results with the H1 tunings appear consistently low throughout the entire kinematic region.

6.4.2 ARIADNE and LEPTO

From fig. 19, as before, we notice that the MEPS model from LEPTO 6.1 is unable to provide sufficient energy in the forward region throughout the kinematic range, and additionally - particularly at low x - the current region is too hard.

Both ARIADNE and LEPTO 6.3 however appear to provide a satisfactory description with perhaps LEPTO 6.3 providing slightly too little in the forward region, most noticably at small x.

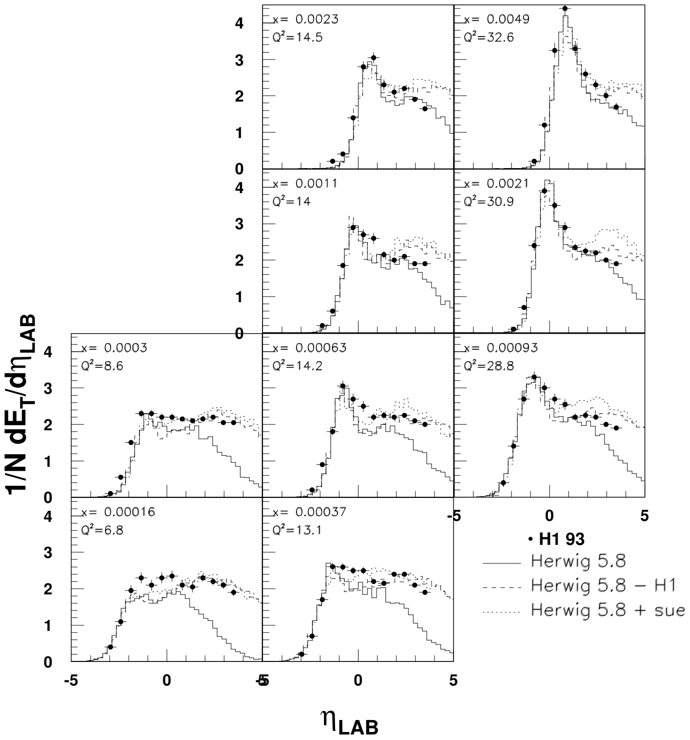

Figure 17: Transverse energy flows in the lab frame for H1 1993 data [40, 41] compared to HERWIG 5.8. All generated using the MRSD-' structure functions

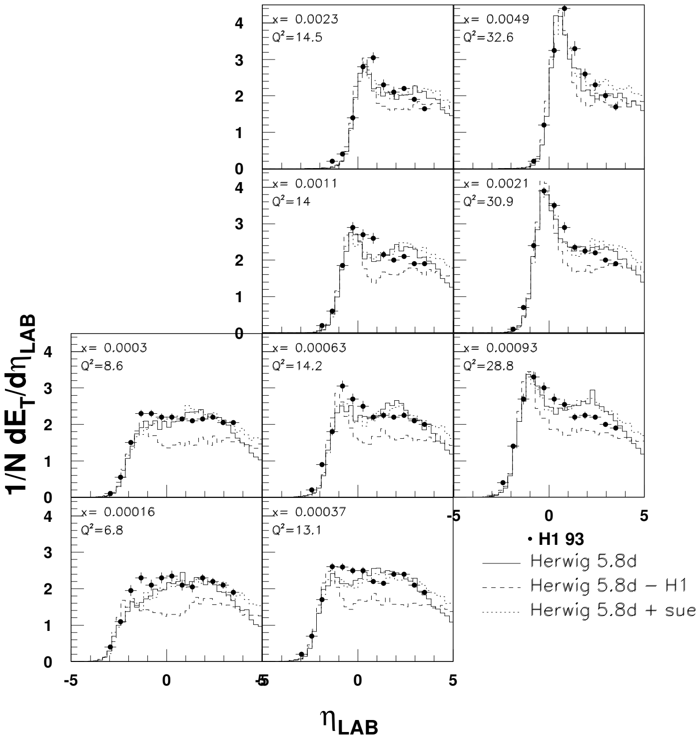

Figure 18: Transverse energy flows in the lab frame for H1 1993 data compared to HERWIG 5.8d. All generated using the MRSD-' structure functions

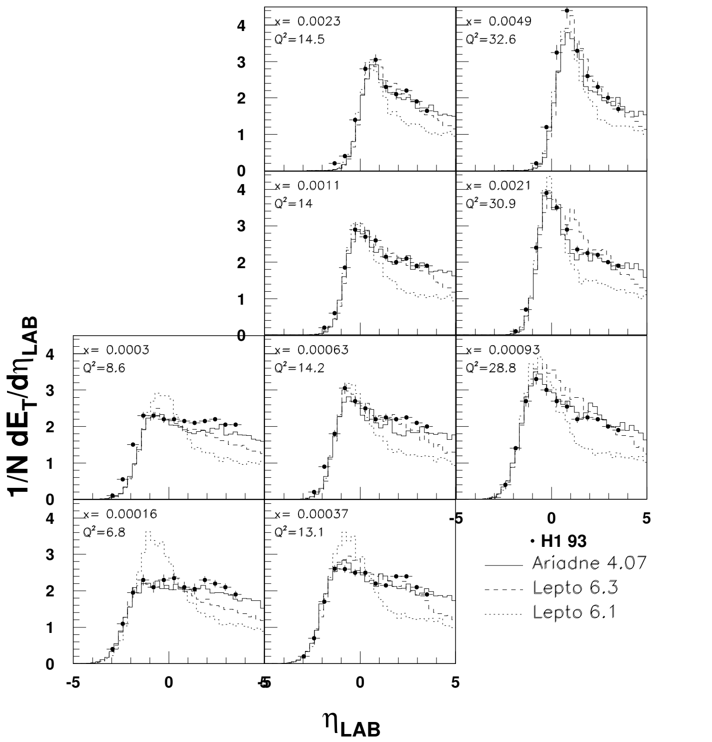

Figure 19: Transverse energy flows in the lab frame for H1 1993 data compared to ARIADNE and LEPTO

6.5 Comparison with ZEUS 94 Data

For the 1994 analysis [42] the ZEUS collaboration considered 24 bins spread over most of the accessible kinematic region of the $x - Q^2$ plane. These bins are shown in figure 20 and besides the limits imposed by the kinematic bins themselves, the

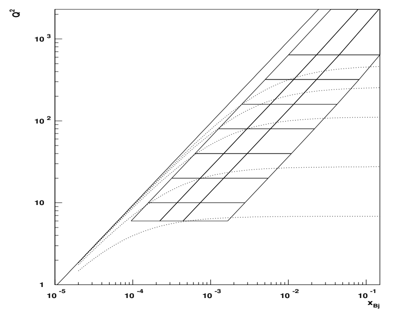

Figure 20: Kinematic bins for the ZEUS 1994 Transverse Energy Flow Analysis

data were unfolded back to the non-diffractive hadronic level with an additional cut

- $x_{\text{pom}} > 10^{-2}$

where x_{pom} can be considered as the momentum fraction of the "pomeron" within the proton in a diffractive event. As such it is given simply by

$$x_{\text{pom}} = \frac{M_X^2 + Q^2}{W^2 + Q^2} \tag{78}$$

where M_X^2 is the invariant mass of the hadronic state resulting from the scattering of the photon from the colour singlet pomeron which can therefore be separated from the remnant by a large gap in rapidity. Gap events are then characterised by a small value of x_{pom}, with $\log x_{\text{pom}}$ being approximately linearly related to η_{max} such that the ZEUS 1993 cut $\eta_{\text{max}} > 1.5$ corresponds approximately to

$x_{\text{pom}} > 10^{-2}$. This value is found to exclude diffractive events without excluding a sizable compoment of the normal DIS data sample [42]. The relationship between x_{pom} and $\eta_{\max}$ is shown in figure 21b. Here we also examine (figure 21a) the effect

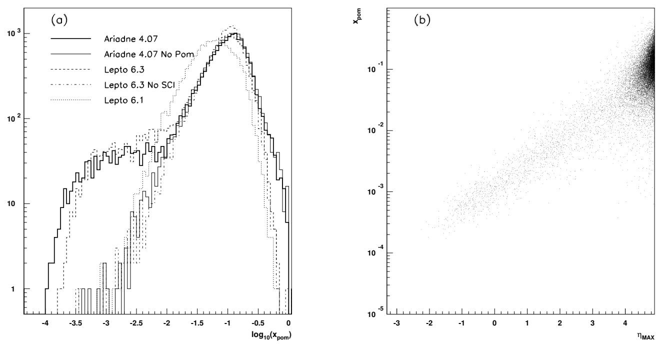

Figure 21: (a) A comparison of the x_{pom} distribution from ARIADNE 4.07 (CDM+BGF) with and without pomeron scattering and LEPTO 6.3 (MEPS) with and without soft colour interactions; (b) Relationship between x_{pom} and $\eta_{\max}$ from LEPTO 6.3 with soft colour interactions.

of the pomeron scattering mechanism within ARIADNE by comparison of the x_{pom} distribution generated with ARIADNE both with and without pomeron scattering, with that of LEPTO 6.1 which includes no mechanism for generating diffractive events and has an x_{pom} spectrum which is much lower at low values of x_{pom}. This clearly shows the effect of the the Pomeron and SCI mechanisms, and the use of the $x_{\text{pom}} > 10^{-2}$ cut in excluding diffractive events.

This should be compared with LEPTO 6.3 which, as mentioned, contains soft colour interactions as an alternative mechanism to generate the diffractive component. The x_{pom} spectra both with and without soft colour interactions clearly demonstrates that this mechanism compares favourably with that of pomeron scattering in this simple test.

Whereas the H1 collaboration used a bin-by-bin correction in their analysis of the 1993 data, the ZEUS data presented here were unfolded using a more sophisticated matrix unfolding method [38, 42] and hence extend beyond the geometrical acceptance of the ZEUS Forward Calorimeter (FCAL), albeit with correspondingly larger systematic uncertainties.

6.5.1 HERWIG

Figures 22 and 23 show 8 of the lowest Q^2 bins arranged for comparison with the (almost) equivalent H1 bins of the previous section. As in the case of the H1 93 data we see that the default 5.8 is unable to provide sufficient energy in the forward region for the lowest x and Q^2 bins. However this is also the case throughout the rest of these low Q^2 bins where the presence of the soft underlying event does much better, although the current region does not appear well treated.

HERWIG 5.8d with default parameters in contrast appears to treat the current region better without the SUE particularly in the low x bins. Also the forward region is well treated over all except in the region beyond the geometric detector acceptance in the lowest x bins where the use of the SUE appears to do a little better, although in this case the current region becomes a little too soft.

Again the use of the H1 parameters produce an E_T flow which is consistently too soft. even in the current region.

6.5.2 ARIADNE and LEPTO

Here again LEPTO 6.1 gives results which are too soft in the forward region and a current region which is badly described, particularly at low x. At higher x both ARIADNE and LEPTO 6.3 do not do so well in the current region, doing better at lower x. Again there also appears a much better agreement between ARIADNE and the new LEPTO in the forward region except in the lowest Q^2 bins where LEPTO appears lower than ARIADNE which seems rather low in comparison with the data.

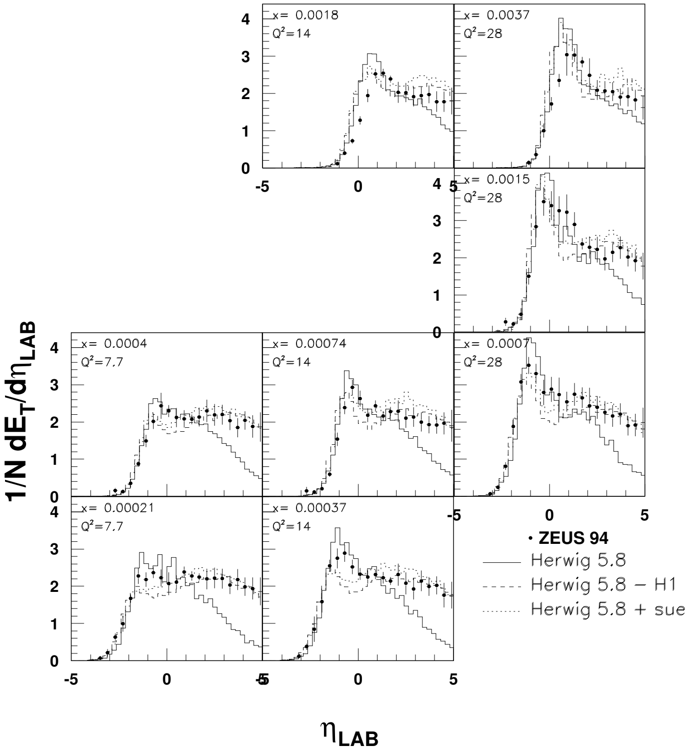

Figure 22: Transverse energy flows in the lab frame for ZEUS 94 [42] data compared to HERWIG 5.8. (MRSD-' structure functions)

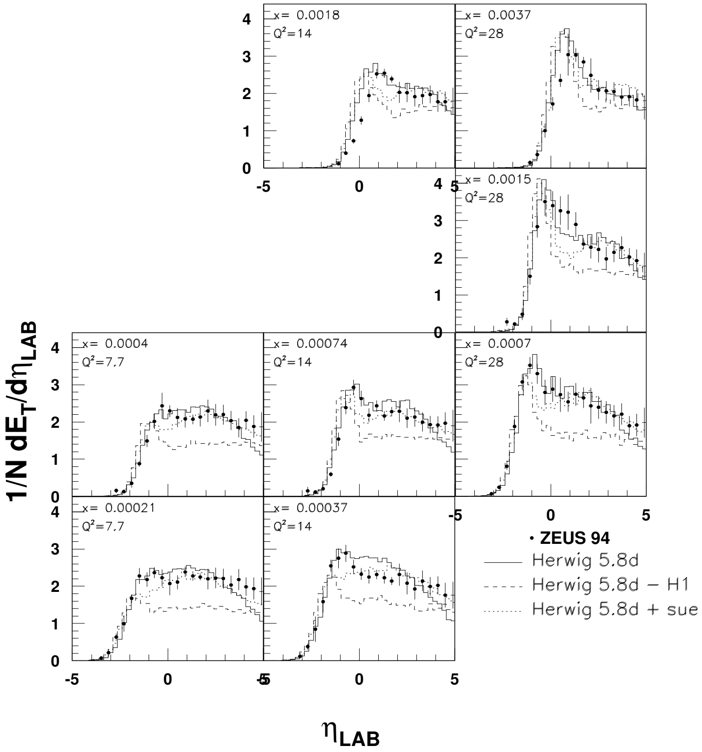

Figure 23: Transverse energy flows in the lab frame for ZEUS 94 data [42] compared to HERWIG 5.8d. (MRSD-' structure functions)

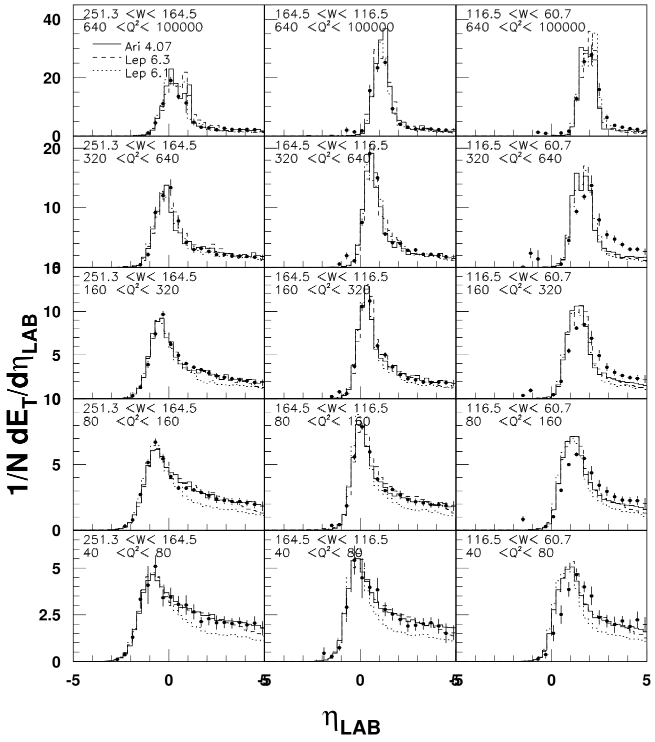

Figure 24: Transverse energy flows in the lab frame for ZEUS 94 data [42] compared to ARIADNE and LEPTO

6.6 The Transverse Energy Flow at Larger Q^2

Figures 25, 26 and 27 show the performance of the Monte Carlos at higher Q^2 and clearly demonstrate that at high Q^2 and intermediate y all the Monte Carlos appear to do well, even LEPTO 6.1, which is too be expected, as in this region we epect the behaviour to be dominated by the fragmentation of the current jet, which we would expect to be well described by traditional DGLAP dynamics.

All five versions also appear to provide a good description of the current region in the largest two y intervals, however as before we notice that HERWIG 5.8 without the SUE is consistently low in the forward region except at high Q^2. This should be contrasted with the default HERWIG 5.8d which appears to do better in this region except in the lowest Q^2 bin shown here. In fact except for the lowest y bins and the lowest Q^2 bins HERWIG 5.8d appears to do well, in bothe the currecnt and the forward regions.

Again ARIADNE seems to provide a good description throughout the kinematic range shown, except at low y were the current region is not particularly well described, and the forward E_T appears a little low in some of the bins. However, here we should notice that the Monte Carlos do appear to agree better, all failing to a greater or lesser extent in this region, particularly at intermediate Q^2.

Consequently it appears that at higher Q^2, when y is not too small, the current region appears reasonably well treated by all the models.

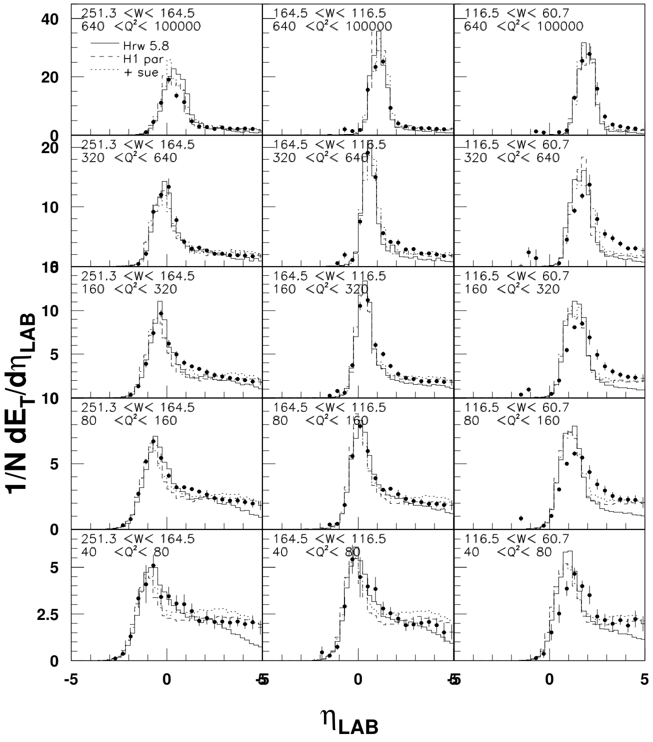

Figure 25: Transverse energy at high Q^2 for ZEUS 94 [42] data compared to HERWIG 5.8. (MRSD-' structure functions)

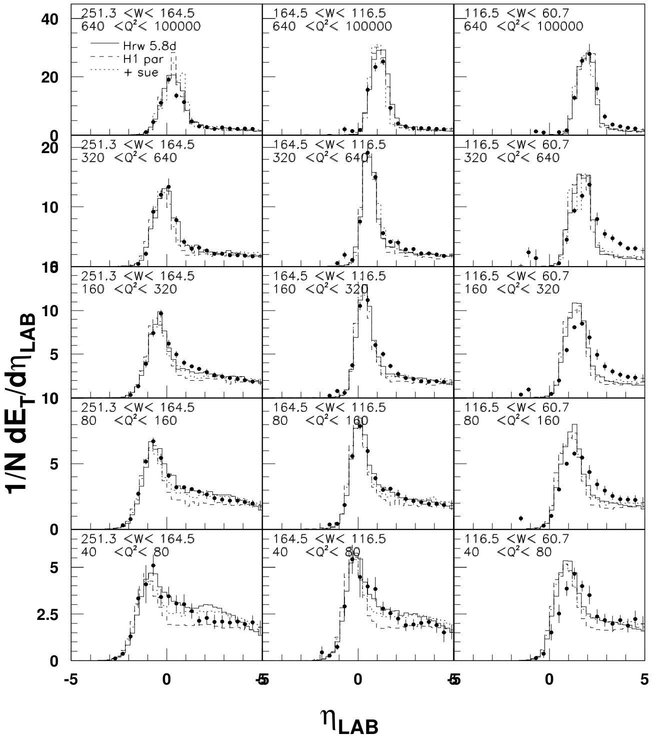

Figure 26: Transverse energy at high Q^2 for ZEUS 94 data [42] compared to HERWIG 5.8d. (MRSD-' structure functions)

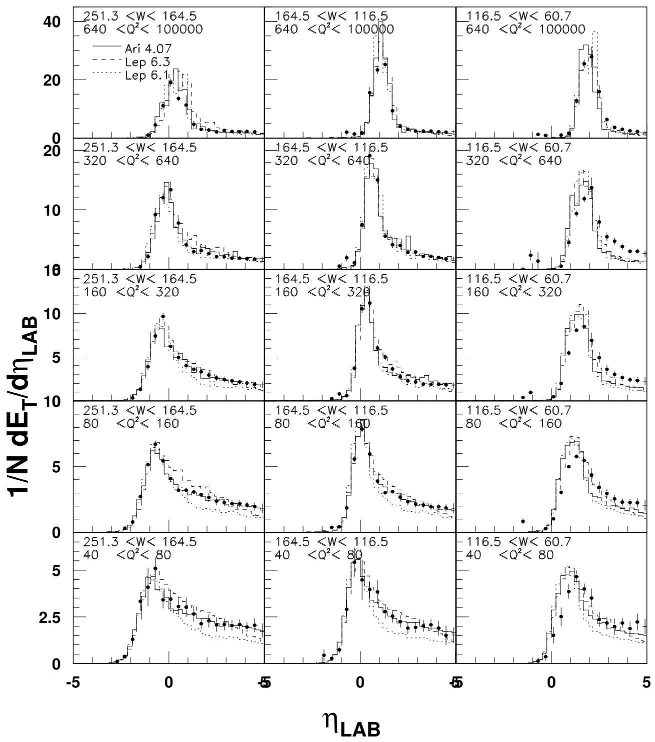

Figure 27: Transverse energy at high Q^2 for ZEUS 94 data [42] compared to ARIADNE and LEPTO

6.7 Energy Flow as a Function of x

With the larger number of kinematic bins it is possible to study the variation of the transverse energy flow with x. This is show for the H1 1993 data in figure 28 and for the ZEUS 1994 data in fig. 29 which show the average value of the non-diffractive E_T in a region $-0.5 < \eta^* < 0.5$ where η^* is the pseudo rapidity in the hadronic centre of mass (HCM). In this frame this region corresponds to the "middle" of the central region with $\eta \to -\infty$ corresponding to the direction of the proton remnant and $\eta \to \infty$ corresponding to the direction of the struck quark in the quark parton model. As the data seem to favour HERWIG 5.8 with

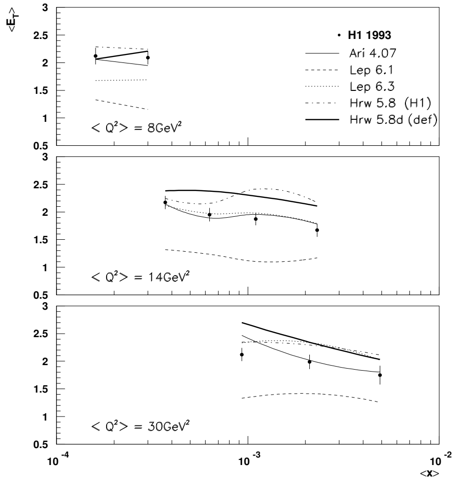

Figure 28: Mean central E_T against x for H1 93 data [41].

the H1 tunings, I compare this with the other Monte Carlos rather than using the defaults 5.8 tunings.

Figure 28 clearly shows the old LEPTO consistentlty providing too little E_T in the central region, with the new LEPTO fairing much better in the central Q^2 region, but still being too low at lower x abnd Q^2, and too high in the higher Q^2 bins. ARIADNE appears to do well in all bins and HERWIG 5.8 with the H1 tunings is doing well at lower x, but is too high at higher x. HERWIG 5.8d does better at low x but, like LEPTO 6.3 appears too high at larger x.

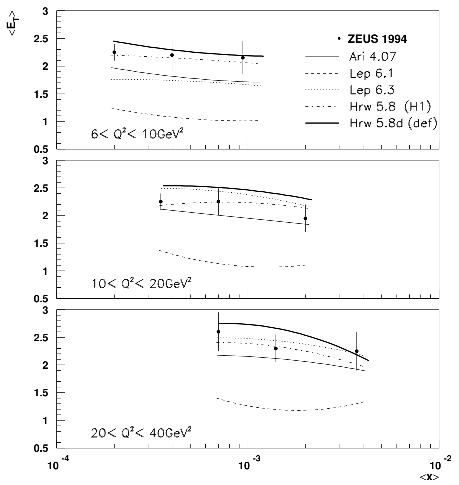

Figure 29: Mean central E_T against x for ZEUS 94 data [42].

In fig. 29 we again see LEPTO 6.1 being consistently low, however, here version 6.3 also appears a little too low in the lower Q^2 bin, and ARIADNE also appears consistently low. In contrast Herwig 5.8d appears to do well in each Q^2 region, with 5.8 with the H1 tunings also doing well. For comparison, in [41] the H1 collaboration also show the results of a BFKL motivated parton level calculation by Askew *et al* in the lowest two Q^2 bins. This does not include any correction

for parton showering or hadronisation and lies approximately 0.5 GeV below the data. It is thought that the effect of including a hadronisation correction will be to increase the level of the BFKL calculation such that it is consistent with the data [26].

Clearly, the new versions of the Monte Carlo, all seem to agree much better and compare better with the data.

7 Conclusion

In conclusion, we see that none of the Monte Carlos studied are able to provide an adequate description of the current or forward regions at low y for the whole range of Q^2 accesible at HERA. However the new versions of LEPTO, ARIADNE and HERWIG do seem to be in closer agreement, except in the lowest x and Q^2 bins of the H1 1993 and ZEUS 1994 analysis where either ARIADNE or HERWIG 5.8d respectively seem to do better.

It seems clear that the new version of HERWIG is now able to provide a reasonable description of the forward energy without the need for the soft underlying event, with the difference obtained including this feature being small except in the very far forward region beyond the geometrical detector acceptance.

It should also be noted that the soft colour interactions of LEPTO 6.3 appear to be able to explain the presence of diffractive events without the need for the pomeron, although a more detailed study of the diffractive region would be required to establish anything more concrete.

Finally it is important to note that now both HERWIG and LEPTO - both Monte Carlos motivated by a traditional DGLAP leading log treatment of the initial state radiation - are able to explain the level of transverse energy flow at small x reasonably well. This is in a region where we would not expect this to be the case. However, it is clear that in this region the fragmentation of the proton remnant may have an important part to play and consequently it may be the case that we do not know yet enough about the remnant fragmentation to be able to unambiguously observe BFKL type behaviour in the forward energy flow observable at current HERA energies and with the current detector configurations. Perhaps with the coming of a BFKL inspired Monte Carlo, upgrades to the HERA detectors, and an increased understanding of the detectors' performance by, for instance, mapping dead material in the forward region using shifted vertex runs and so on we may be able to reduce the systematic errors and extend the detector ascceptance to improve the situation.

8 Acknowledgements

I would like to thank Tegid, Phil, Nick Brook, PPARC and so on, and I think that that's about it for the acknowledgements for this this type of report.

References

[1] M. Gell-Mann; Phys. Lett **8** (1964) 214.
G. Zweig; CERN Rep. 8182/TH 401.

[2] F. Halzen and A.D. Martin; "Quarks and Leptons", Wiley (1984).
R.G. Roberts; "The Structure of the Proton" Cambridge University Press (1990).
D. Griffiths; "Introduction to Elementary Particles" Wiley, (1987).
A. Bailin and D. Love; "Introduction to Gauge Field Theory" Institute of Physics (1990).

[3] C.G. Callan and D. Gross; Phys. Rev. Lett. **22** (1969) 156.

[4] J.I. Friedman and H.W. Kendall; Annual Review of Nucl. and Particle Science, Vol. 22 (1972) 227.

[5] E. Berger and S. Brodsky; Phys. Rev. Lett. **42** (1979) 940.
E. Berger; Z. Phys. **C4** (1980) 289.

[6] D.J. Gross and F. Wilczek, Phys. Rev. lett. **30** (1973) 1343; Phys. Rev. **D8** (1973) 3633;
H.D. Politzer, Phys. Rev. Lett. **30** (1973) 1346.

[7] G. Alterelli and G. Parisi; Nucl. Phys. **B126** (1977) 298.

[8] T. Kinoshita; J. Math. Phys. **3** (1962) 650;
T.D. Lee and M. Nauenberg; Phys. Rev. **133** (1964) 1549.

[9] F. Bloch and A. Nordsieck, Phys. Rev. **52** (1937) 54.

[10] L.V. Gribov and L.N. Lipatov; Sov. J. Nucl. Phys. **15**(6) (1972) 675: Sov. J. Nucl. Phys. **15**(4) (1972) 438.

[11] J. Kwiecinski, A.D. Martin,W.J. Stirling and R.G. Roberts; Phys. Rev. **D42** (1990) 3645.

[12] L.N. Lipatov; Sov. J. Nucl. Phys. **23**(3) (1976) 338.
Ya. Ya. Balitskii and L.N. Lipatov; Sov. J. Nucl. Phys. **28**(6) (1978) 822.
E.A. Kuraev, L.N. Lipatov and V.S. Fadin; Sov. Phys. JETP **45**(2) (1977) 199.

[13] A. Donnachie and P.V. Landshoff; Manchester University Preprint M/C-TH 93/11; DAMTP preprint DAMTP 93-23.

[14] E.M. Levin and M.G. Ryskin; Phys. Rep. **189** (1990) 269.

[15] M. Glück, E. Reya and A. Vogt; Phys. Lett. **B306** (1993) 391.

[16] CTEQ Collaboration; Phys. Lett. **B304** (1993) 159.

[17] S. Bentvelsen, J. Engelen and P. Kooijman in "Physics at HERA" edited by W. Buchmuller and G. Ingelman. (Proceedings of the workshop, Hamburg, October 1991), Vol 1 p.23.

[18] J. Bartels; J. Phys. G **19** (1993) 1611.

[19] J.R. Forshaw, P.N. Harriman and and P.J. Sutton; Nucl. Phys. **B416** (1994) 739.

[20] J.R. Forshaw, P.N. Harriman and and P.J. Sutton; J. Phys. G **19** (1993) 1616.

[21] A.J. Askew, J. Kwiecinski, A.D. Martin and P.J. Sutton; Phys. Rev. **D49** (1994) 4402. (Durham Preprint DTP/93/28.)

[22] A.D. Martin, W.J. Stirling and R.G. Roberts; Phys. Rev. **D47** (1993) 867.

[23] A.J. Askew, K. Golec-Biernat, J. Kwiecinski, A.D. Martin and P.J. Sutton; Phys. Rev. **D47** (1993) 3775: Phys. Lett. **B325** (1994) 212. (Preprint IFJ 1653/PH.)

[24] H1 Collaboration; Nucl. Phys. **B407** (1993) 515.
ZEUS Collaboration; Phys. Lett. **B316** (1993) 412.

[25] J. Kwiecinski, A.D. Martin, P.J. Sutton and K. Golec-Biernat; Phys. Rev. **D50** (1994) 217.

[26] K. Golec-Biernat, J. Kwiecinski, A.D. Martin and P.J. Sutton; Durham Preprint DTP/94/30 (1994).

[27] A.D. Martin, W.J. Stirling and R.G. Roberts; Phys. Lett. **B306** (1993) 145.

[28] G. Ingelman; "Physics at HERA" edited by W. Buchmuller and G. Ingelman. (Proceedings of the workshop, Hamburg, October 1991), Vol 3 p1366(???).

[29] G. Ingelman, J. Rathsman, A. Edin; DESY note 95 (1995) ISSN 0418-9833.

[30] G. Ingelman, J. Rathsman, A. Edin; DESY note 95-163 (1995).

[31] G. Gustafson; Phys. Lett. **B175** (1986) 453.
G. Gustafson and U. Pettersson; Nucl. Phys. **B175** (1988) 453.
B. Andersson, G. Gustafson and L. Lönnblad; Nucl. Phys. **B339** (1990) 393.

[32] L. Lönnblad; Comput. Phys. Commun. **71** (1992) 15.

[33] T. Sjöstrand; Comput. Phys. Commun. **82** (1994) 74; PYTHIA 5.7 and JETSET 7.4 Physics and Manual, CERN-TH.7112/93, Dec 1993,(revised Aug. 1994)

[34] B. Andersson, G. Gustafson, G. Ingelman and T. Sjöstrand; Phys. Rep. **97** (1983) 33.

[35] G. Marchesini, B.R. Webber, G. Abbiendi, I.G. Knowles, M.H. Seymour and L.Stanco; Comp. Phys. Commun. **67** (1992) 465.

[36] G. Abbiendi; ZEUS Note 95-099 (August 1995).

[37] M. Seymour; "Mike's Herwig Information page", WWW currently `http://surya11.cern.ch/users/seymour/herwig`.

[38] T. Haas and P.B. Kaziewicz; ZEUS note ZEUS-95-017 (1994).

[39] H1 Collaboration; DESY preprint DESY-94-033 (1994).

[40] T. Haas; ZEUS note ZEUS-95-051 (1995).

[41] H1 Collaboration; DESY note DESY-95-108.

[42] P.B. Kaziewicz; PhD. Thesis "Energy Flows in Deep Inelastic Scattering at HERA" University College London (1995).